Carrier Generation and Collection in CdS/CdSe-Sensitized SnO_2 Solar Cells Exhibiting Unprecedented Photocurrent Densities

Md. Anower Hossain, James Robert Jennings, Zhen Yu Koh, and Qing Wang*

Department of Materials Science and Engineering, Faculty of Engineering, NUSNNI-NanoCore, National University of Singapore, Singapore 117576

ABSTRACT CdS/CdSe-sensitized nanostructured SnO_2 solar cells exhibiting record short-circuit photocurrent densities have been fabricated. Under simulated AM 1.5, 100 mW cm^{-2} illumination, photocurrents of up to 17.40 mA cm^{-2} are obtained, some 32% higher than that achieved by otherwise identical semiconductor-sensitized solar cells (SSCs) employing nanostructured TiO_2. An overall power conversion efficiency of 3.68% has been achieved for the SnO_2-based SSCs, which compares very favorably to efficiencies obtained by the TiO_2-based SSCs. The characteristics of these SSCs were studied in more detail by optical measurements, spectral incident photon-to-current efficiency (IPCE) measurements, and impedance spectroscopy (IS). The apparent conductivity of sensitized SnO_2 photoanodes is apparently too large to be measured by IS, yet for otherwise identical TiO_2 electrodes, clear electron transport features could be observed in impedance spectra, tacitly implying slower charge transport in TiO_2. Despite this, electron diffusion length measurements suggest that charge collection losses are negligible in both kinds of cell. SnO_2-based SSCs exhibit higher IPCEs compared with TiO_2-based SSCs which, considering the similar light harvesting efficiencies and the long electron diffusion lengths implied by IS, is likely to be due to a superior charge separation yield. The resistance to charge recombination is also larger in SnO_2-based SSCs at any given photovoltage, and open-circuit photovoltages under simulated AM 1.5, 100 mW cm^{-2} illumination are only 26–56 mV lower than those obtained for TiO_2-based SSCs, despite the conduction band minimum of SnO_2 being hundreds of millielectronvolts lower than that of TiO_2.

KEYWORDS: semiconductor-sensitized solar cell · tin oxide · cadmium selenide · charge separation · charge collection · diffusion length

Semiconductor nanocrystals, especially quantum dots (QDs), have been attracting considerable attention due to their potential use as sensitizers in sensitized mesoscopic solar cells.[1,2] The ease with which the band gap can be tuned by varying particle size,[3] and other inherent absorption properties, makes QDs very promising candidates for efficient light harvesting materials in this type of solar cells.[4,5] In recent years, a lot of work on QD-sensitized solar cells has been reported where sensitization was achieved using CdS,[6−11] CdSe,[12−14] or PbS[15−18] and in some cases co-sensitization using more than one of these materials. In most reports, nanocrystalline TiO_2 is used as the photoanode.[19−21] The highest efficiencies of semiconductor-sensitized solar cells (SSCs) reported in the past few years are in the range of 4−5%.[22−24]

Nanostructured SnO_2 is known to have higher electron mobility than nanostructured TiO_2[25,26] and also a much more negative conduction band minimum (CBM).[1,18,27] Exploitation of the low CBM of SnO_2 should facilitate charge transfer from low band gap sensitizers such as near-infrared light absorbers, PbS,[1,17] PbSe,[28] and $CuInSe_2$,[29] *etc.*, where light harvesting could be significantly enhanced by utilizing long wavelength photons. Therefore, nanostructured SnO_2 is an interesting photoanode material, which could in principle facilitate efficient charge injection and charge collection. While the photovoltaic conversion efficiencies for cells employing SnO_2 are notoriously poor in dye-sensitized solar cells, it shows great promise in SSCs.[30]

It has been shown that the photoconversion efficiency of a QD-sensitized solar cell can be enhanced by co-sensitization of CdS and CdSe in a layered structure of TiO_2/CdS/CdSe, where the band edges of the three materials form a stepwise cascade, which is advantageous in the separation of excited electrons and holes across the interfacial region.[22,31−34] In our study, layers of semiconductors (CdS/CdSe/ZnS) were coated conformally onto SnO_2 by the successive ionic layer adsorption and reaction method (SILAR).[22,31−36] A passivation layer of TiO_2 on the SnO_2 surface is necessary before deposition of CdS in order to reduce the density of electron trap states at the surface of SnO_2. Likewise, a barrier layer of ZnS, deposited by a post-treatment onto the core−shell CdS/CdSe, is required to inhibit the recombination of injected electrons with holes in the electrolyte, as investigated in a previous publication.[30]

* Address correspondence to qing.wang@nus.edu.sg.

Received for review January 25, 2011 and accepted March 8, 2011.

Published online March 08, 2011
10.1021/nn200315b

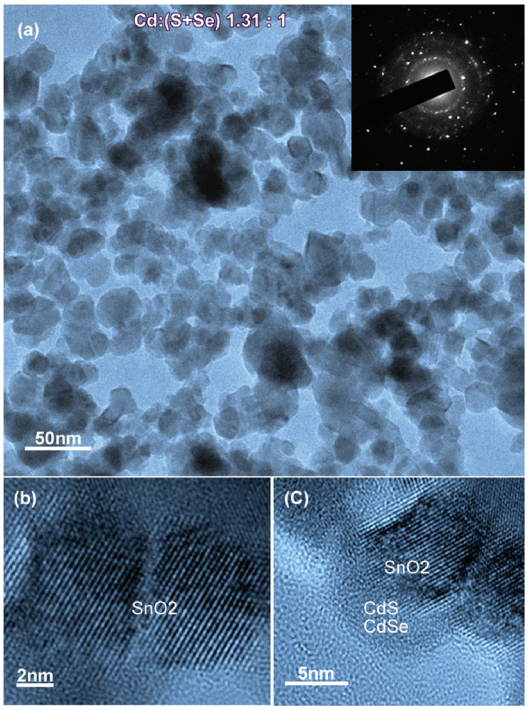

Figure 1. TEM image of a SnO_2/CdS/CdSe electrode (a), HRTEM image of SnO_2 grains (b), and conformal coating of CdS/CdSe onto SnO_2 (c).

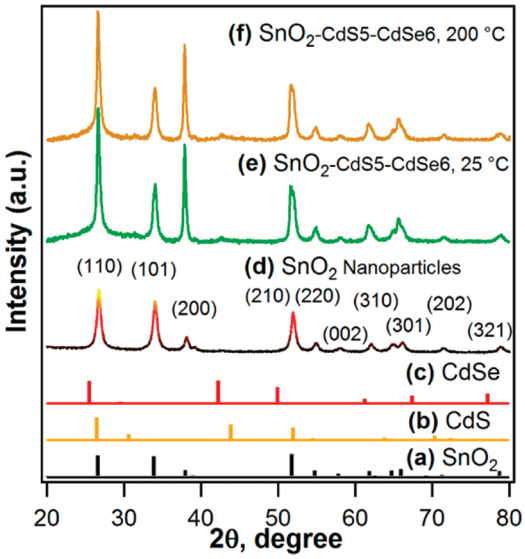

Figure 2. X-ray diffraction patterns of reference SnO_2 nanoparticles (a), CdS thin film (b), CdSe thin film (c) and measured diffraction patterns of SnO_2 nanoparticles (d), an untreated CdS/CdSe-coated SnO_2 sample (e), and after sintering in vacuum for 6 h at 200 °C (f).

In this article, attempts to improve the photocurrent of SSCs by using SnO_2 as a photoanode instead of TiO_2 are described. Basic $j-V$, incident photon-to-current conversion efficiency (IPCE), and optical measurements have been combined with impedance spectroscopy (IS) in order to scrutinize charge generation, transport, and recombination in these SSCs. Ultimately, a record photocurrent density of 17.40 mA cm^{-2} was obtained under simulated AM 1.5, 100 mW cm^{-2} illumination when an aqueous polysulfide electrolyte and a Cu_2S cathode were used. The maximum IPCE was observed to be close to 80% over a wide wavelength range, indicating almost unity quantum efficiency, after correction for light absorption by the FTO substrate. On the other hand, for TiO_2-based SSCs, a maximum IPCE of only 65% was obtained which, based upon results of IS, is thought to be due to inferior charge separation as opposed to charge collection. Very promising overall power conversion efficiencies of up to 3.68% were achieved, making nanostructured SnO_2 a potential rival to TiO_2 for use in SSCs.

RESULTS AND DISCUSSION

Morphology and Structural Examination. Figure 1a shows a TEM image of CdS/CdSe-coated SnO_2 nanoparticles (5/5 SILAR cycles, *cf.* Experimental Section), with approximate sizes in the range of 20−40 nm. High-resolution transmission electron microscopy (HRTEM) suggests that these SnO_2 particles consist of crystal grains of ∼12 nm (Figure 1b,c). Energy-dispersive X-ray spectroscopy (EDS) elemental analysis shows the existence of Cd, S, and Se. The atomic ratio Cd:(S+Se) was found to be 1.31:1, indicating that the layer as a whole was Cd-rich and broadly consistent with previous reports where Cd-rich CdSe was deposited by SILAR.[14] A conformal coating of CdS/CdSe on the SnO_2 was revealed by HRTEM (Figure 1c), and the lack of lattice fringes suggests the as-grown sensitizer is amorphous.

The crystal structure of samples was characterized by powder X-ray diffraction (XRD). As shown in Figure 2d, the XRD pattern revealed that the SnO_2 nanoparticles are polycrystalline, consistent with the HRTEM image (Figure 1b,c), which shows lattice fringes with *d* spacing of 0.335 nm, corresponding to the lattice plane (110) of tetragonal rutile SnO_2 (JCPDS No. 41-1445, Figure 2a). The calculated grain size of ∼12 nm from the Scherrer equation using the first and second peaks (Figure 2d) was consistent with the grain size obtained from analysis of HRTEM images. Additional features due to CdS and CdSe were not observed in the X-ray diffraction analysis, except for a noisier profile (Figure 2e,f), arising because of the amorphous nature of the conformal coating of CdS/CdSe.

Optical Properties of CdS/CdSe-Sensitized SnO_2 Electrodes. Nanocrystalline CdS and CdSe are widely used semiconductor sensitizers for nanocrystalline TiO_2 solar cells because their composite absorption spectrum covers most of the visible region.[22,31,37] The SILAR method offers the easiest way to deposit semiconductor absorber layers onto nanocrystalline electrodes, where mostly the coating is conformal. Co-sensitization by core−shell quantum dots yields important absorption properties and charge separation characteristics, which depend on the relative band positions of the constituent sensitizer materials.[30]

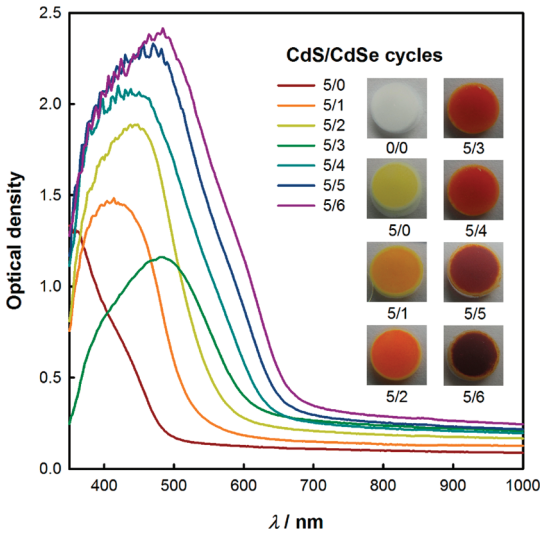

Figure 3. UV−vis optical density spectra of CdS and CdS/CdSe-coated SnO_2 electrodes alongside typical photographs of electrodes with or without five cycles of CdS and different numbers of CdSe cycles.

Figure 3 shows optical density (OD) spectra of a 6.4 μm thick SnO_2 electrode as it is coated with CdS/CdSe by successive SILAR cycles. The incorporated amount of CdS or CdSe into the SnO_2 films increases with increasing numbers of SILAR cycles. As shown in Figure 3, the apparent absorption onset of five-cycle CdS/SnO_2 electrodes occurs at ~500 nm, representing its bulk nature and optical band gap of 2.50 eV.[38] Successive color changes from yellow ochre (5/1) to dark red (5/6) were observed with the increase of CdSe deposition cycles (inset of Figure 3), indicating strong absorption of most of the visible wavelengths.

For all spectra, an apparent absorbance extending up to 1000 nm was observed which systematically increases with the number of SILAR deposition cycles. We suspect this is due to uncorrected light scattering losses which increase with increasing CdS/CdSe coverage; rigorous corrections for light scattering using diffuse transmittance and reflectance measurements have not yet been attempted. Despite the ambiguities caused by scattering effects, it still seems very reasonable to assume that the light harvesting efficiency of the sensitized electrodes is almost unity in the wavelength range of 400−500 nm, where an OD of >2 is found for *ca.* 6 μm thick electrodes (note that the electrodes used in complete SSCs were 9 μm thick). The same conclusion can be drawn for TiO_2 electrodes sensitized with 5/5 CdS/CdSe SILAR cylcles, which have similar OD spectra (Supporting Information).

A deviation in the magnitude of OD was also observed for the specific case of a 5/3 combination of CdS/CdSe, where the absorption onset followed the trend of the other films, but the peak absorption was less than for 5/2 and 5/4 CdS/CdSe combinations. This surprising result was reproducible; adding an additional CdSe cycle to a 5/2 electrode resulted in a *decrease* in peak OD together with the expected extension of the absorption onset to longer wavelengths. Since the detailed composition and morphology of these CdS/CdSe layers is unknown, we do not wish to speculate about the origin of this peculiar phenomenon, which is the subject of ongoing investigation in our laboratory.

These co-sensitized electrodes have wide wavelength absorption characteristics, emphasizing that the main sensitization comes from CdSe, due to its wider spectral response than CdS. Likewise, due to size-induced electronic quantization phenomena, the absorption onset of CdS/CdSe-sensitized electrodes moves to longer wavelengths with the increase of CdSe deposition cycles, indicating the increment of the thickness of the CdSe layer. The performance of SSCs incorporating CdS/CdSe-sensitized electrodes has been studied, and the optimum layer combination is found to be 5/5 CdS/CdSe. It should be mentioned that the samples of SnO_2/CdS/CdSe used for OD measurements were prepared without $TiCl_4$ pretreatment of the SnO_2 electrodes or the ZnS post-treatment. It has been reported that the ZnS layer decreases quantum confinement and red shifts the spectral absorption, but hardly participates in harvesting of incident light itself, rather it plays an important role in improving charge separation and collection.[31]

Photocurrent−Voltage and Energy Conversion Characteristics. To study the photovoltaic performance of CdS/CdSe-sensitized mesoscopic SnO_2 electrodes, sandwich-type thin layer cells were fabricated with FTO/SnO_2/CdS/CdSe as the photoanode, platinized FTO and Cu_2S on brass as the cathode, and a polysulfide electrolyte as the hole transporter. To prevent recombination at the SnO_2/CdS/CdSe/electrolyte interface, SnO_2 electrodes were treated with $TiCl_4$ aqueous solution prior to CdS/CdSe deposition, and a thin passivation layer of ZnS was deposited onto the sensitized electrode by two SILAR deposition cycles.

Figure 4a shows the IPCE spectra of CdS/CdSe-sensitized SnO_2 and TiO_2 solar cells, which exhibit a strong photoresponse over the entire visible light range, with photon wavelengths even extending to ~850 nm for the SnO_2 SSCs. It has been shown that, for the co-sensitized electrode, the higher IPCE in the short-wavelength region is due to the CdS, whereas CdSe harvests light in the long wavelength region; together a better overall IPCE response was observed.[39] IPCEs of ~80% between 400 and 600 nm were achieved with 5/5 layers of CdS/CdSe on SnO_2 and 2 layers of ZnS. Since the IPCE is found to be within a few percent of the transmission of the FTO substrate in this wavelength range, it must be concluded that light harvesting, charge separation, and charge collection are all close to unity when SnO_2 electrodes are used.

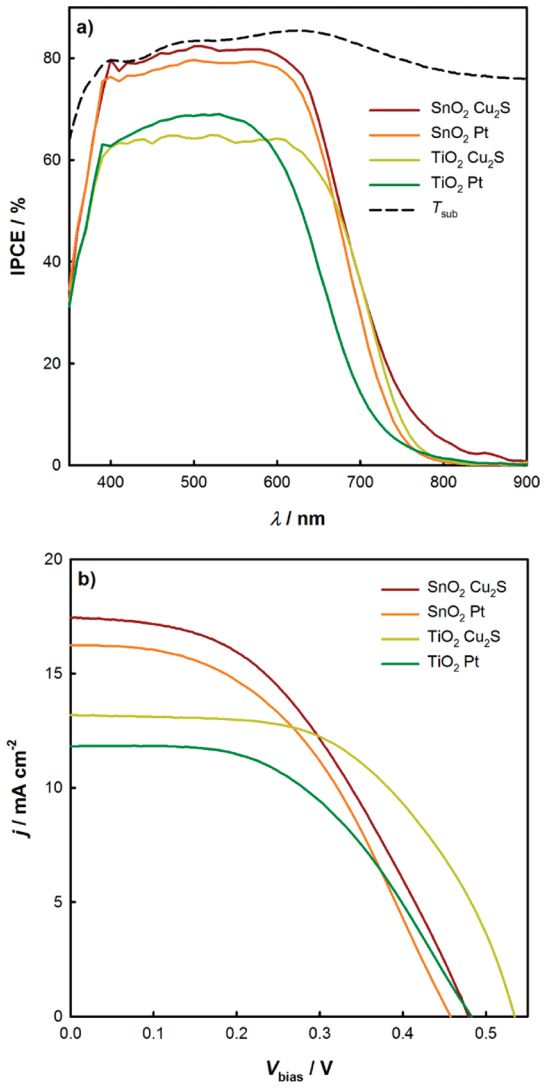

Figure 4. IPCE spectra (a) and *j*−*V* characteristics (b) of CdS/CdSe-sensitized SnO_2 and TiO_2 solar cells.

TABLE 1. Characteristics of CdS/CdSe-Sensitized SnO_2 and TiO_2 Solar Cells with Platinized FTO and Cu_2S Cathodes under Simulated AM 1.5, 100 mW cm^{-2} Illumination

photoanode	CdS/CdSe	cathode	V_{oc} (V)	j_{sc} (mA cm^{-2})	ff (%)	η (%)
SnO_2	5/5	Pt	0.458	16.20	45.85	3.43
	5/5	Cu_2S	0.477	17.40	44.40	3.68
TiO_2	5/5	Pt	0.484	11.82	49.39	2.85
	5/5	Cu_2S	0.533	13.17	55.28	3.88

Figure 4b shows the *j*−*V* characteristics of sensitized SnO_2 and TiO_2 SSCs. Photovoltaic parameters of the SSCs are given in Table 1. As expected from the IPCE measurements, SnO_2 electrodes exhibit superior short-circuit photocurrents as compared to TiO_2 electrodes. The short-circuit photocurrents (j_{sc}) predicted by convolution of IPCE spectra with the AM 1.5 spectrum followed by integration over all wavelengths underestimate the measured 1 Sun j_{sc} values by *ca.* 10%, implying differences in charge separation and charge collection between the IPCE measurements (which were made using low intensity monochromatic illumination) and the 1 Sun *j*−*V* measurements are minimal.

The best SnO_2 device was obtained with 5/5 CdS/CdSe as well as $TiCl_4$ and ZnS pre- and post-treatments, respectively, yielding j_{sc} = 17.4 mA cm^{-2}, V_{oc} = 0.477 V, fill factor = 44.4%, and η = 3.68% under simulated AM 1.5, 100 mW cm^{-2} illumination. One plausible reason for the higher photocurrent of the SnO_2 SSC compared with the TiO_2 SSC is better charge transport dynamics in SnO_2 arising from the higher electron mobility, which will shortly be discussed in the light of results from electrochemical impedance spectroscopy experiments. It is also known that SnO_2 has a much lower conduction band minimum (CBM) than TiO_2 in the same media. The large driving force for charge injection originating from the low CBM of SnO_2 may help efficient charge injection from excited CdS/CdSe to the conduction band of SnO_2. Leventis *et al.* recently reported comparative studies of charge separation between PbS-sensitized mesoscopic TiO_2 and SnO_2.[17] Transient optical measurements showed much faster charge injection for the PbS-sensitized SnO_2 electrode.[17] Guijarro *et al.* have shown that the injection of electrons from CdSe into TiO_2 decreases significantly with increasing numbers of SILAR cycles.[14] This could be eliminated by using a low CBM oxide such as SnO_2 for an electron acceptor material. Pijpers *et al.* have shown efficient electron injection from PbSe into SnO_2; however, there was no injection into TiO_2, which was attributed to the different energy band alignments when using these oxides.[40]

As found previously,[30] a $TiCl_4$ treatment effectively passivates the surface of SnO_2 and significantly improves the photovoltaic performance of CdSe-sensitized SnO_2 solar cells. Prasittichai *et al.* have found that the photovoltaic performance of dye-sensitized SnO_2 solar cells increased 5-fold when the surface was passivated with an ultrathin layer of Al_2O_3, stemming from inhibited recombination.[41] In addition, SILAR deposition forms a conformal coating of CdS and CdSe on SnO_2, which acts as a barrier layer (in a similar way to Al_2O_3), preventing injected electrons in SnO_2 from recombining with holes in the electrolyte. Moreover, it is believed that surface modification by ZnS further inhibits the recombination of excited electrons at the electrode/electrolyte interface and increases the injection from the sensitizer into TiO_2.[42−44]

In this work, optimized TiO_2 SSCs yielded j_{sc} = 13.17 mA cm^{-2}, V_{oc} = 0.533 V, fill factor = 55.28%, and η = 3.88% when Cu_2S cathodes were used. The better overall performance of the TiO_2 cell with the same configuration arises from the higher fill factor and slightly higher V_{oc}, which compensate for the lower photocurrent. When platinized cathodes were used in place of Cu_2S cathodes, performance with both

oxides was found to be lower due to inferior fill factor and j_{sc}. While the photocurrent of CdS/CdSe-sensitized SnO_2 SSCs is significantly higher than the value reported for CdS/CdSe-sensitized TiO_2 cells,[19,22,31] the overall efficiency still remains lower. It is not surprising that the V_{oc} of the SnO_2 cell would be lower than the TiO_2 SSCs because of the low CBM and unchanged redox level of the polysulfide electrolyte, and in fact, a much larger loss in V_{oc} might be expected.

The effect of the SnO_2 mesoporous film thickness on the cell performance was investigated by varying the film thickness from 5.5 to 10.5 μm, with the same CdS/CdSe sensitizer loading. Photocurrents normally increased with film thickness, but V_{oc} and fill factor dropped, eventually leading to a decrease in efficiency for thicknesses >9 μm. For the TiO_2 SSCs, an optimum thickness of ~9 μm was also found.

Investigation of Charge Transport and Recombination Processes Using Impedance Spectroscopy. Impedance spectroscopy (IS) was used to compare the charge transport and charge transfer processes occurring in TiO_2- and SnO_2-based SSCs. Figure 5 shows representative IS spectra for TiO_2- (Figure 5a) and SnO_2-based SSCs (Figure 5b). For the case of the TiO_2-based SSCs, excellent fits to most spectra (dashed red lines in Figure 5a) can be obtained using an equivalent circuit (Supporting Information) based upon the now ubiquitous diffusion-reaction model for a porous electrode, as described by Bisquert.[45]

In spectra recorded for TiO_2-based SSCs, for photovoltages in the range of 0.1−0.3 V, a clear Warburg-like feature can be observed, which is consistent with previous reports and can be assigned to electron diffusion in the TiO_2 layer.[22] The associated electron transport resistance (R_t) decreases as open-circuit photovoltage (V_{oc}) becomes increasingly more negative, corresponding to the electron quasi-Fermi level rising toward the CBM and the free carrier concentration in the semiconductor increasing. The slope on a semilogarithmic plot of R_t *versus* V_{oc} (dashed black line in Figure 5c) is 16.6 V^{-1}, which is in good agreement with the theoretical value of 17 V^{-1} at 295 K, lending support to the assignment of the Warburg-like impedance feature to the electron transport process.

On the contrary, for the SnO_2-based SSCs, no high-frequency Warburg-like feature is observed under any conditions (*cf.* Figure 5b), and excellent fits to the data can be obtained with a simplified equivalent circuit consisting of the series connection of a resistor and two parallel RC circuits. One RC circuit represents the SnO_2 layer (with negligible resistance to electron transport), and the other represents the cathode−electrolyte interface. This finding implies that the electron transport resistance for these cells is always much lower than the cathode impedance; if this were not the case, it ought to be apparent in the impedance spectrum. Consequently, the electron diffusion length in these cells is expected to be exceedingly long compared with the SnO_2 layer thickness.

A crude estimate of the minimum electron diffusion length at the cell voltage of the maximum power point (V_{mpp}) for the SnO_2-based SSC can be made by taking the SnO_2 interfacial charge transfer resistance (R_{ct}) at a photovoltage corresponding to V_{mpp} and assuming the electron transport resistance (R_t) is equal to the cathode charge transfer resistance (probably a gross overestimation). This approach yields L_n of the order of 10 times the SnO_2 layer thickness, implying a collection efficiency of practically unity, regardless of optical considerations. This estimate is entirely consistent with the IPCE spectra for SnO_2-based SSCs employing Cu_2S cathodes, where IPCE values approaching the substrate transmission are found (*cf.* Figure 4a).

Attempts were made to more precisely estimate L_n at various photovoltages by using a combination of intensity-modulated photovoltage spectroscopy (IMVS) and intensity-modulated photocurrent spectroscopy (IMPS). However, ultimately, this was not possible because under all conditions studied (open-circuit, various light intensities) the IMPS response was found to be dominated by the RC time constant of the cells and deconvolution of the transport time constant with any reasonable degree of accuracy was impossible.

Attempts were also made to observe electron transport features in the IS spectra by using a Cu_2S electrode to reduce the impedance of the cathode. However, due to the instability of the Cu_2S cathodes used in this work (which were fabricated by reaction of a brass substrate with the electrolyte), interpretation of impedance spectra were complicated by non-negligible drift of the system on the time scale of the measurements (which typically took 1−2 h), thus further analysis will not be presented here. However, it is noteworthy that, in these experiments, features in the impedance spectra (*e.g.*, slope of ~1 in Nyquist plots) which were clearly attributable to an electron transport resistance were not observed.

For the TiO_2-based SSCs, long electron diffusion lengths are also found for V_{oc} > 0.2 V, where L_n is greater than 3 times the TiO_2 layer thickness, sufficient to ensure almost 100% efficient charge collection, regardless of illumination direction and absorption coefficient.[46] Below V_{oc} = 0.2 V, L_n decreases into a regime where charge collection losses could begin to become a photocurrent loss mechanism (the extent of which will depend upon the precise absorption coefficient of the sensitized metal oxide layer and on the illumination direction). However, this exceptionally low quasi-Fermi level position (obtained

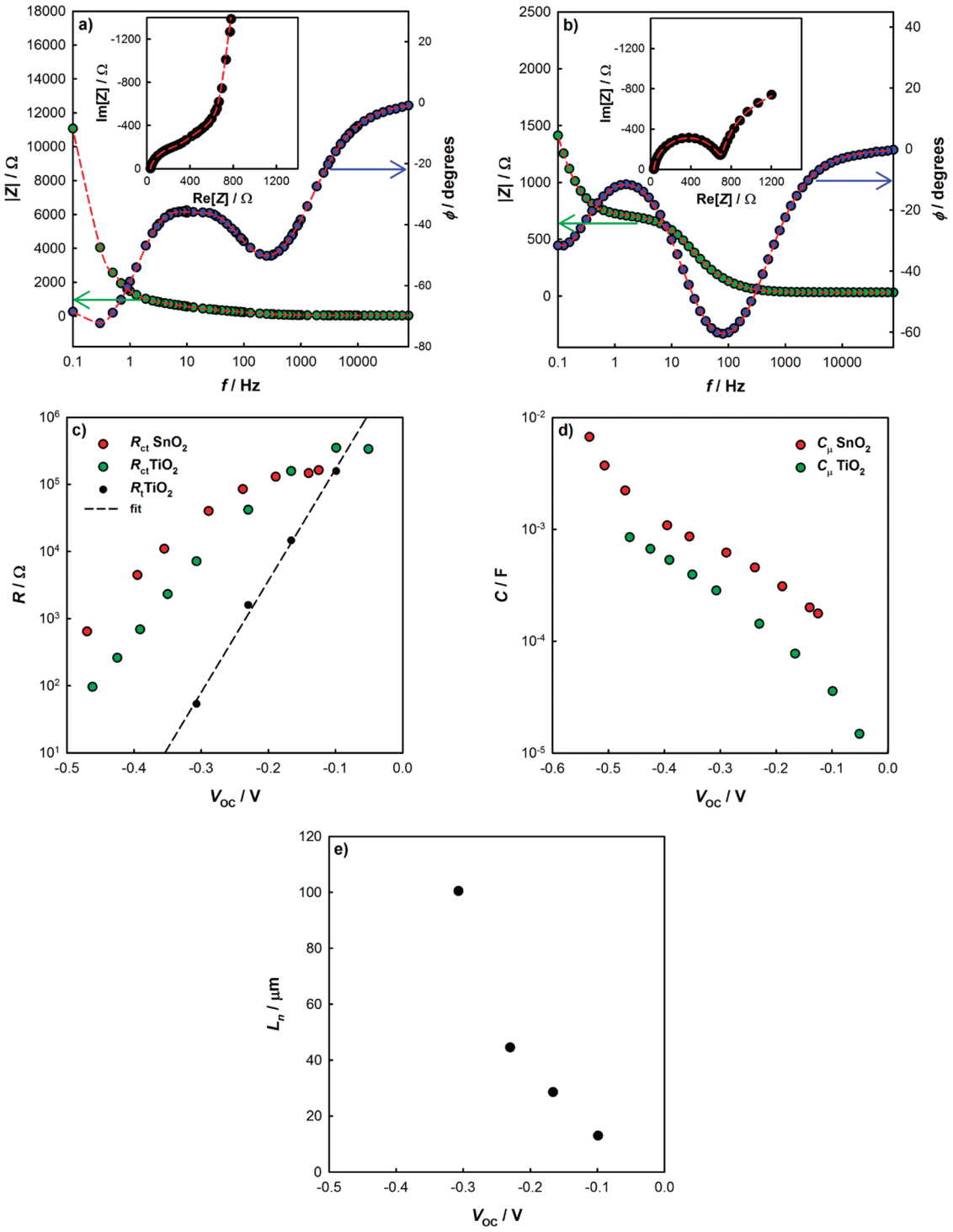

Figure 5. Bode and Nyquist plots showing typical IS results and best fits using the diffusion-reaction model (dashed red lines) for TiO_2- (a; $V_{oc} = -0.23$ V, incident photon flux *ca.* 3×10^{14} cm^{-2} s^{-1}, $\lambda = 627$ nm) and SnO_2- (b; $V_{oc} = -0.19$ V, incident photon flux *ca.* 3×10^{14} cm^{-2} s^{-1}, $\lambda = 627$ nm) based SSCs; charge transfer resistance and transport resistance (c), and chemical capacitance (d) parameters obtained from fitting; dependence of electron diffusion length derived from IS fitting results on open-circuit photovoltage for a TiO_2-based SSC (e).

under very low incident light intensity) is unlikely to be encountered in the device under normal 1 Sun operating conditions, where the average quasi-Fermi level in the bulk of the metal oxide layer for cell voltages below V_{mpp} (*e.g.*, short-circuit) is expected to be only 0.15−0.25 V lower than V_{oc} at the same light intensity.[47−49] It is noteworthy that the electron mobility in single crystal rutile SnO_2[25] is *ca.* 10 times higher than in single-crystal anatase TiO_2,[26] and it is possible that this is a factor contributing to the conspicuous absence of a prominent Warburg feature in the IS spectra for SnO_2-based SSCs, despite

it being observed for otherwise identical TiO_2-based SSCs.

Peak IPCE and j_{sc} values for SnO_2-based SSCs are around 30−40% higher than for TiO_2-based SSCs. Upon the basis of the diffusion length estimations for the TiO_2-based device, it appears unlikely that this difference can be explained by charge collection losses in the TiO_2-based SSCs. This is because, despite the apparently superior transport properties of SnO_2 compared with TiO_2, transport is still *fast enough* to avoid collection losses in the TiO_2-based SSCs. Assuming that differences in light harvesting efficiency between SnO_2 and TiO_2 electrodes are not significant over most of the absorbed wavelength range (this assumption is supported by transmission measurements for λ = 400 to at least λ = 500 nm; Supporting Information), it is likely that the cause for higher IPCE and photocurrent is that the overall charge separation yield in SnO_2-based SSCs is higher than in TiO_2-based SSCs. Since identical electrolytes and sensitizer deposition procedures were used for both types of SSC, it must be concluded that either charge injection from the CdS/CdSe to the metal oxide is slower in the TiO_2 system compared to the SnO_2 system, or that the reverse process, geminate recombination, is faster in the TiO_2 system.

The CBM of SnO_2 is thought to lie 0.3−0.5 eV below that of anatase TiO_2, and therefore, on purely energetic grounds, a higher charge injection efficiency might be expected. However, one must also consider that use of Marcus−Gerischer electron transfer theory is probably more appropriate for predicting the probability of electron transfer from the semiconductor sensitizer to the metal oxide. In this case, the density of acceptor states at the relevant energy (the energy of the excited states of CdS/CdSe) in the metal oxide is more important than the free energy difference between initial and final states in the charge transfer process.

The conventional interpretation of the porous electrode capacitance obtained from IS data using the diffusion-reaction model is that it corresponds to a chemical capacitance, that is, a measure of the effective density of states around the quasi-Fermi level, which, in turn, is related to V_{oc} by $V_{oc} = {}_nE_F - E_{F,redox}$. Since identical electrolytes were used in both types of SSC, comparisons of C_μ at matched V_{oc} ought to reveal differences between the densities of states in the two oxides, on an energy reference scale relevant to the operation of these cells. Figure 5d clearly shows that, at any given V_{oc}, C_μ for the SnO_2-based device is at least 2 times larger than for the TiO_2-based device, and at lower voltages is almost 4 times larger. Thus, if it is permissible to extrapolate these results to the energies relevant to charge injection, the higher IPCE values for the SnO_2-based SSCs compared with the TiO_2 counterparts may be due to enhanced electron injection, as a result of the higher density of electron acceptor states at the appropriate energy. The shift along the voltage axis between the two plots in Figure 5d might also be viewed as evidence that the SnO_2 layer has a lower conduction band minimum than TiO_2, as expected. However, since the density of states functions for the two materials are not known and are unlikely to be the same, quantifying the difference in band edge energies is not possible without more information.

It is also interesting to note that the charge transfer resistance (R_{ct}) for the SnO_2-based SSC is up to 6 times larger than that for the TiO_2-based SSC. At very low photovoltages, similar R_{ct} values are found, but data obtained at these photovoltages are not likely to be relevant to normal operation of the cells. The larger R_{ct} is a factor that contributes toward the surprisingly high photovoltages achieved by the SnO_2-based SSCs, which are only 26−56 mV lower than for TiO_2-based SSCs, despite the far more positive CBM of SnO_2. However, it must also be borne in mind that the effective density of states at the CBM (N_C), together with the energy of the CBM, determines the free electron concentration required to produce a particular quasi-Fermi level position and V_{oc}. The effective electron mass in SnO_2 is reported to be *ca.* 35 times smaller than estimates for nanocrystalline TiO_2,[50,51] thus significant differences in N_C between the two materials probably exist, and the relatively small difference in V_{oc} between the cells cannot be solely attributed to slower charge recombination in the SnO_2-based SSCs.

CONCLUSIONS

CdS/CdSe-sensitized SnO_2 solar cells exhibiting record photocurrent densities of up to 17.40 mA cm^{-2} under simulated AM 1.5, 100 mW cm^{-2} illumination have been fabricated. Consistent with the high photocurrent, an IPCE of close to 80% over almost the entire visible spectral region is observed, also implying highly efficient charge separation and collection. Open-circuit photovoltage is similar to that obtained by TiO_2-based SSCs, despite the much more positive CBM of SnO_2. Impressive overall power conversion efficiencies of up to 3.68% were achieved, making nanostructured SnO_2 a rival to TiO_2 for use in SSCs.

A detailed comparison between SnO_2 and TiO_2 photoanodes reveals SnO_2 can be considered a superior material to TiO_2 in many respects, owing to higher recombination resistances, faster charge transport, and more efficient charge separation. However, the efficiency of SSCs employing SnO_2 may be limited by the relatively low conduction band energy compared with TiO_2. To overcome this problem, we anticipate

that control of surface dipoles at the various interfaces (*e.g.*, SnO_2/CdS, ZnS/electrolyte, *etc.*) will be important in engineering band edge positions with respect to the electrolyte redox level and consequently improving V_{oc}. Another strategy to improve conversion efficiency might involve replacement of the polysulfide electrolyte with one possessing a more positive redox potential; however, this approach will almost certainly lead to changes in sensitizer regeneration rate and charge recombination rate, which may or may not be beneficial to device performance.

EXPERIMENTAL SECTION

Preparation of Mesoscopic SnO_2 Electrodes. Tin(IV) oxide (SnO_2) nanoparticles (Alfa Aesar, Nanoarc) mixed with a small amount of ethanol were ground by pestle and mortar to break up agglomerates. Ethyl cellulose and α-terpineol were then mixed with the ground SnO_2 powder following a previously reported procedure for making TiO_2 paste.[52] SnO_2 electrodes were prepared by screen-printing the above paste onto FTO glass (TEC, 15 Ω/□) several times in order to get an appropriate thickness. The printed films were then sintered in air by heating gradually to 325 °C and holding for 5 min, then 375 °C for 5 min, at 450 °C for 15 min, and finally at 500 °C for 15 min. The resulting mesoporous SnO_2 electrodes were semi-transparent. The thickness of the electrodes was determined by an Alpha-Step IQ surface profiler to be ~9 μm. After preparation, SnO_2 electrodes were immersed into 40 mM aqueous $TiCl_4$ solution at 70 °C for 40 min and then washed with water and ethanol followed by drying in an electric oven at 70 °C.

Preparation of CdS/CdSe-Sensitized Mesoscopic SnO_2 Electrodes. After masking the bare FTO with Kapton tape, leaving the mesoscopic SnO_2 electrodes (6 mm diameter) uncovered, they were sensitized with CdS and CdSe using previously reported SILAR methods.[19,22,30] In a typical procedure, the SnO_2 electrodes were immersed in a solution containing 0.02 M cadmium nitrate tetrahydrate ($Cd(NO_3)_2 \cdot 4H_2O$, Fluka, >99.0%) in methanol for 1 min, to allow Cd^{2+} to adsorb onto the SnO_2, and then rinsed with methanol for 1 min to remove the excess Cd^{2+}. Electrodes were then dried in a gentle stream of N_2 for 1 min. The dried electrodes were then dipped into a solution containing 0.02 M sodium sulfide nonahydrate ($Na_2S \cdot 9H_2O$, Sigma Aldrich) in a mixture of methanol and deionized water (1:1, v/v) for 1 min, where the preadsorbed Cd^{2+} reacts with S^{2-} to form the desired CdS. Electrodes were then rinsed in methanol for 1 min and dried again with N_2. This procedure was repeated five times in order to get a suitable CdS loading on the SnO_2 electrode. CdSe was also deposited onto the CdS-coated SnO_2 electrodes by the SILAR method, where they were dipped into a solution containing 0.03 M cadmium nitrate tetrahydrate ($Cd(NO_3)_2 \cdot 4H_2O$, Fluka, >99.0%) in ethanol for 30 s and rinsed with ethanol for 2 min, then dried for 2 min in an argon atmosphere. Subsequently, the dried electrodes were dipped in to a solution containing 0.03 M Se^{2-} for 30 s. The Se^{2-} solution was prepared by mixing selenium dioxide (SeO_2, Sigma-Aldrich, 99.9%) and sodium borohydride ($NaBH_4$, Sigma Aldrich) in ethanol following the work reported by Lee *et al.*[19] One deposition cycle was completed by further rinsing in ethanol for 2 min and drying again in an argon atmosphere for 2 min. This procedure was repeated several times to get suitable CdSe loading on CdS-coated SnO_2 electrodes. A ZnS passivation layer was deposited on a CdS/CdSe-coated SnO_2 electrode by SILAR using 0.1 M aqueous zinc acetate dihydrate ($Zn(CH_3COO)_2 \cdot 2H_2O$, Sigma Aldrich, >99.5%) and 0.1 M aqueous $Na_2S \cdot 9H_2O$, dipping for 1 min in each solution, with 1 min of rinsing in deionized water between each immersion in a precursor solution. All the CdS/CdSe-sensitized SnO_2 electrodes used in this study were coated with two ZnS passivation layers. For comparison, TiO_2 electrodes were prepared by screen-printing TiO_2 paste (Degussa P25 powder and ethyl cellulose in α-terpineol) on bare FTO to produce ~9 μm thick layers. The rest of the fabrication procedure was identical to that used for CdS/CdSe-sensitized SnO_2 electrodes.

Material Characterization. Powder X-ray diffraction (XRD) measurements of SnO_2 nanoparticles and SnO_2/CdS/CdSe electrodes were carried out with a Bruker D8 using Cu Kα1 radiation (λ = 0.154059 nm). The detailed morphology of the SnO_2 particles were elucidated from transmission electron microscopy on JEOL JEM 2010F, which also facilitated energy-dispersive X-ray analysis (EDX). Samples for TEM investigations were prepared by detaching the CdS/CdSe-sensitized SnO_2 nanocrystals mechanically from the FTO glass substrate and dispersing in ethanol, followed by transferring one drop of the suspension onto a carbon-coated copper grid. Optical density/transmission spectra were collected using a Shimadzu UV−vis−NIR spectrophotometer (Solidspec-3700) at room temperature.

Fabrication and Characterization of CdS/CdSe-Sensitized SnO_2 Solar Cells. Platinized counter electrodes were fabricated on FTO with small holes drilled into one corner. After cleaning, a thin layer of Pt was deposited onto the FTO by thermal decomposition of hexachloroplatinic acid. Brass foil (alloy 260, Alfa Aesar) was also used to prepare Cu_2S counter electrodes.[53,54] Brass foil was etched in 37% HCl at 70 °C for 5 min to expose more copper from the copper−zinc matrix, and the yellowish color of the brass changed to a dark red. The etched brass was then rinsed with deionized water and dried at 70 °C. One drop of an aqueous polysulfide solution containing 1 M S and 1 M $Na_2S \cdot 9H_2O$ was added onto an unmasked part of the etched brass, causing it to suddenly become black, indicating the formation of Cu_2S. To fabricate SSCs with brass cathodes, a hole was made within 1 mm from the edge of the SnO_2 layer on the photoanode. Photoanodes and cathodes were sealed together in a sandwich configuration using a hot-melt polymer (Surlyn, DuPont). The interelectrode space was filled with an electrolyte by vacuum backfilling. Holes were sealed using a small piece of hot-melt polymer and a microscope coverslip. The electrolyte was composed of 1 M S, 1 M $Na_2S \cdot 9H_2O$, and 0.1 M NaOH in deionized water. IPCE spectra were measured with a spectral resolution of *ca.* 5 nm using a 300 W xenon lamp and a grating monochromator equipped with order sorting filters (Newport/Oriel). The incident photon flux was determined using a calibrated silicon photodiode (Newport/Oriel). Photocurrents were measured using an autoranging current amplifier (Newport/Oriel). Control of the monochromator and recording of photocurrent spectra were performed using a PC running the TRACQ Basic software (Newport). Current−voltage characteristics under simulated AM 1.5 illumination were measured using a Keithley Source Meter and the PVIV software package (Newport). Simulated AM 1.5 illumination was provided by a Newport class A solar simulator, and light intensity was measured using a calibrated Si solar cell. The active area of the cells was defined by a mask to be 0.1199 cm^2. V_{oc} intensity characteristics and IS spectra were measured using an Autolab potentiostat/galvanostat and the Nova 1.6 software package. IS experiments were performed with cells under illumination provided by a red LED (center wavelength λ = 627 nm) and biased at the V_{oc} induced by the illumination. The highest light intensity used was sufficient to produce a V_{oc} approximately equal to that obtained under AM 1.5 1 Sun illumination, and the incident photon flux was of the order of 10^{17} cm^{-2} s^{-1}. A 15 mV rms voltage perturbation was used, and the frequency range was 10^5 to 0.1 Hz. Different illumination intensities were achieved using neutral density filters mounted in an automated filter wheel system (Newport), which was controlled by the Nova 1.6 software.

Acknowledgment. This work was financially supported by NUS startup Grant No. R-284-000-064-133, URC Grant No. R-284-000-068-112, and NRF CRP Grant No. R-284-000-079-592.

Supporting Information Available: Optical characteristics of CdS/CdSe-sensitized TiO_2 electrodes (Figure S1) and equivalent circuit used for analysis of impedance spectra (Figure S2). This material is available free of charge *via* the Internet at http://pubs.acs.org.

REFERENCES AND NOTES

1. Vogel, R.; Hoyer, P.; Weller, H. Quantum-Sized PbS, CdS, Ag_2S, Sb_2S_3, and Bi_2S_3 Particles as Sensitizers for Various Nanoporous Wide-Bandgap Semiconductors. *J. Phys. Chem.* **1994,** *98*, 3183–3188.
2. Nozik, A. J. Quantum Dot Solar Cells. *Physica E* **2002,** *14*, 115–120.
3. Yu, W. W.; Qu, L.; Guo, W.; Peng, X. Experimental Determination of the Extinction Coefficient of CdTe, CdSe, and CdS Nanocrystals. *Chem. Mater.* **2003,** *15*, 2854–2860.
4. Kongkanand, A.; Tvrdy, K.; Takechi, K.; Kuno, M.; Kamat, P. V. Quantum Dot Solar Cells. Tuning Photoresponse through Size and Shape Control of CdSe-TiO_2 Architecture. *J. Am. Chem. Soc.* **2008,** *130*, 4007–4015.
5. Kamat, P. V. Quantum Dot Solar Cells. Semiconductor Nanocrystals as Light Harvesters. *J. Phys. Chem. C* **2008,** *112*, 18737–18753.
6. Gopidas, K. R.; Bohorquez, M.; Kamat, P. V. Photophysical and Photochemical Aspects of Coupled Semiconductors: Charge-Transfer Processes in Colloidal Cadmium Sulfide−Titania and Cadmium Sulfide−Silver(I) Iodide Systems. *J. Phys. Chem.* **1990,** *94*, 6435–6440.
7. Peter, L. M.; Riley, D. J.; Tull, E. J.; Wijayantha, K. G. U. Photosensitization of Nanocrystalline TiO_2 by Self-Assembled Layers of CdS Quantum Dots. *Chem. Commun.* **2002,** 1030–1031.
8. Lin, S.-C.; Lee, Y.-L.; Chang, C.-H.; Shen, Y.-J.; Yang, Y.-M. Quantum-Dot-Sensitized Solar Cells: Assembly of CdS-Quantum-Dots Coupling Techniques of Self-Assembled Monolayer and Chemical Bath Deposition. *Appl. Phys. Lett.* **2007,** *90*, 143517-3.
9. Robel, I.; Subramanian, V.; Kuno, M.; Kamat, P. V. Quantum Dot Solar Cells. Harvesting Light Energy with CdSe Nanocrystals Molecularly Linked to Mesoscopic TiO_2 Films. *J. Am. Chem. Soc.* **2006,** *128*, 2385–2393.
10. Shalom, M.; Dor, S.; Rühle, S.; Grinis, L.; Zaban, A. Core/CdS Quantum Dot/Shell Mesoporous Solar Cells with Improved Stability and Efficiency Using an Amorphous TiO_2 Coating. *J. Phys. Chem. C* **2009,** *113*, 3895–3898.
11. Sun, W.-T.; Yu, Y.; Pan, H.-Y.; Gao, X.-F.; Chen, Q.; Peng, L.-M. CdS Quantum Dots Sensitized TiO_2 Nanotube-Array Photoelectrodes. *J. Am. Chem. Soc.* **2008,** *130*, 1124–1125.
12. Lee, Y.-L.; Huang, B.-M.; Chien, H.-T. Highly Efficient CdSe-Sensitized TiO_2 Photoelectrode for Quantum-Dot-Sensitized Solar Cell Applications. *Chem. Mater.* **2008,** *20*, 6903–6905.
13. Leschkies, K. S.; Divakar, R.; Basu, J.; Enache-Pommer, E.; Boercker, J. E.; Carter, C. B.; Kortshagen, U. R.; Norris, D. J.; Aydil, E. S. Photosensitization of ZnO Nanowires with CdSe Quantum Dots for Photovoltaic Devices. *Nano Lett.* **2007,** *7*, 1793–1798.
14. Guijarro, N. s.; Lana-Villarreal, T.; Shen, Q.; Toyoda, T.; Gómez, R. Sensitization of Titanium Dioxide Photoanodes with Cadmium Selenide Quantum Dots Prepared by SILAR: Photoelectrochemical and Carrier Dynamics Studies. *J. Phys. Chem. C* **2010,** *114*, 21928–21937.
15. Plass, R.; Pelet, S.; Krueger, J.; Grätzel, M.; Bach, U. Quantum Dot Sensitization of Organic−Inorganic Hybrid Solar Cells. *J. Phys. Chem. B* **2002,** *106*, 7578–7580.
16. Lee, H.; Leventis, H. C.; Moon, S.-J.; Chen, P.; Ito, S.; Haque, S. A.; Torres, T.; Nüesch, F.; Geiger, T.; Zakeeruddin, S. M.; *et al.* PbS and CdS Quantum Dot-Sensitized Solid-State Solar Cells: "Old Concepts, New Results". *Adv. Funct. Mater.* **2009,** *19*, 2735–2742.
17. Leventis, H. C.; O'Mahony, F.; Akhtar, J.; Afzaal, M.; O'Brien, P.; Haque, S. A. Transient Optical Studies of Interfacial Charge Transfer at Nanostructured Metal Oxide/PbS Quantum Dot/Organic Hole Conductor Heterojunctions. *J. Am. Chem. Soc.* **2010,** *132*, 2743–2750.
18. Hyun, B.-R.; Zhong, Y.-W.; Bartnik, A. C.; Sun, L.; Abruña, H. D.; Wise, F. W.; Goodreau, J. D.; Matthews, J. R.; Leslie, T. M.; Borrelli, N. F. Electron Injection from Colloidal PbS Quantum Dots into Titanium Dioxide Nanoparticles. *ACS Nano* **2008,** *2*, 2206–2212.
19. Lee, H.; Wang, M.; Chen, P.; Gamelin, D. R.; Zakeeruddin, S. M.; Grätzel, M.; Nazeeruddin, M. K. Efficient CdSe Quantum Dot-Sensitized Solar Cells Prepared by an Improved Successive Ionic Layer Adsorption and Reaction Process. *Nano Lett.* **2009,** *9*, 4221–4227.
20. Li, G. S.; Zhang, D. Q.; Yu, J. C. A New Visible-Light Photocatalyst: CdS Quantum Dots Embedded Mesoporous TiO_2. *Environ. Sci. Technol.* **2009,** *43*, 7079–7085.
21. Lee, H. J.; Chen, P.; Moon, S.-J.; Sauvage, F.; Sivula, K.; Bessho, T.; Gamelin, D. R.; Comte, P.; Zakeeruddin, S. M.; Seok, S. I.; *et al.* Regenerative PbS and CdS Quantum Dot Sensitized Solar Cells with a Cobalt Complex as Hole Mediator. *Langmuir* **2009,** *25*, 7602–7608.
22. González-Pedro, V.; Xu, X.; Mora-Seró, I. n.; Bisquert, J. Modeling High-Efficiency Quantum Dot Sensitized Solar Cells. *ACS Nano* **2010,** *4*, 5783–5790.
23. Fan, S. Q.; Fang, B.; Kim, J. H.; Kim, J. J.; Yu, J. S.; Ko, J. Hierarchical Nanostructured Spherical Carbon with Hollow Core/Mesoporous Shell as a Highly Efficient Counter Electrode in CdSe Quantum-Dot-Sensitized Solar Cells. *Appl. Phys. Lett.* **2010,** *96*, 063501.
24. Chang, J. A.; Rhee, J. H.; Im, S. H.; Lee, Y. H.; Kim, H.-j.; Seok, S. I.; Nazeeruddin, M. K.; Gratzel, M. High-Performance Nanostructured Inorganic−Organic Heterojunction Solar Cells. *Nano Lett.* **2010,** *10*, 2609–2612.
25. Jarzebski, Z. M.; Marton, J. P. Physical Properties of SnO_2 Materials. *J. Electrochem. Soc.* **1976,** *123*, 299C–310C.
26. Forro, L.; Chauvet, O.; Emin, D.; Zuppiroli, L.; Berger, H.; Levy, F. High Mobility n-Type Charge Carriers in Large Single Crystals of Anatase (TiO_2). *J. Appl. Phys.* **1994,** *75*, 633–635.
27. Grätzel, M. Photoelectrochemical Cells. *Nature* **2001,** *414*, 338–344.
28. Leschkies, K. S.; Beatty, T. J.; Kang, M. S.; Norris, D. J.; Aydil, E. S. Solar Cells Based on Junctions between Colloidal PbSe Nanocrystals and Thin ZnO Films. *ACS Nano* **2009,** *3*, 3638–3648.
29. Castro, S. L.; Bailey, S. G.; Raffaelle, R. P.; Banger, K. K.; Hepp, A. F. Nanocrystalline Chalcopyrite Materials ($CuInS_2$ and $CuInSe_2$) *via* Low-Temperature Pyrolysis of Molecular Single-Source Precursors. *Chem. Mater.* **2003,** *15*, 3142–3147.
30. Hossain, M. A.; Yang, G.; Parameswaran, M.; Jennings, J. R.; Wang, Q. Mesoporous SnO_2 Spheres Synthesized by Electrochemical Anodization and Their Application in CdSe-Sensitized Solar Cells. *J. Phys. Chem. C* **2010,** *114*, 21878–21884.
31. Lee, H. J.; Bang, J.; Park, J.; Kim, S.; Park, S.-M. Multilayered Semiconductor (CdS/CdSe/ZnS)-Sensitized TiO_2 Mesoporous Solar Cells: All Prepared by Successive Ionic Layer Adsorption and Reaction Processes. *Chem. Mater.* **2010,** *22*, 5636–5643.
32. Niitsoo, O.; Sarkar, S. K.; Pejoux, C.; Rühle, S.; Cahen, D.; Hodes, G. Chemical Bath Deposited CdS/CdSe-Sensitized Porous TiO_2 Solar Cells. *J. Photochem. Photobiol. A* **2006,** *181*, 306–313.
33. Sudhagar, P.; Jung, J. H.; Park, S.; Lee, Y.-G.; Sathyamoorthy, R.; Kang, Y. S.; Ahn, H. The Performance of Coupled (CdS:CdSe) Quantum Dot-Sensitized TiO_2 Nanofibrous Solar Cells. *Electrochem. Commun.* **2009,** *11*, 2220–2224.
34. Chi, C.-F.; Cho, H.-W.; Teng, H.; Chuang, C.-Y.; Chang, Y.-M.; Hsu, Y.-J.; Lee, Y.-L. Energy Level Alignment, Electron Injection, and Charge Recombination Characteristics in CdS/CdSe Cosensitized TiO_2 Photoelectrode. *Appl. Phys. Lett.* **2011,** *98*, 012101-3.

35. Lee, Y. L.; Lo, Y. S. Highly Efficient Quantum-Dot-Sensitized Solar Cell Based on Co-sensitization of CdS/CdSe. *Adv. Funct. Mater.* **2009,** *19*, 604–609.
36. Toyoda, T.; Oshikane, K.; Li, D.; Luo, Y.; Meng, Q.; Shen, Q. Photoacoustic and Photoelectrochemical Current Spectra of Combined CdS/CdSe Quantum Dots Adsorbed on Nanostructured TiO_2 Electrodes, Together with Photovoltaic Characteristics. *J. Appl. Phys.* **2010,** *108*, 114304-7.
37. Buhbut, S.; Itzhakov, S.; Tauber, E.; Shalom, M.; Hod, I.; Geiger, T.; Garini, Y.; Oron, D.; Zaban, A. Built-in Quantum Dot Antennas in Dye-Sensitized Solar Cells. *ACS Nano* **2010,** *4*, 1293–1298.
38. Zhai, T.; Fang, X.; Bando, Y.; Liao, Q.; Xu, X.; Zeng, H.; Ma, Y.; Yao, J.; Golberg, D. Morphology-Dependent Stimulated Emission and Field Emission of Ordered CdS Nanostructure Arrays. *ACS Nano* **2009,** *3*, 949–959.
39. Lee, Y.-L.; Chi, C.-F.; Liau, S.-Y. CdS/CdSe Co-sensitized TiO_2 Photoelectrode for Efficient Hydrogen Generation in a Photoelectrochemical Cell. *Chem. Mater.* **2009,** *22*, 922–927.
40. Pijpers, J. J. H.; Koole, R.; Evers, W. H.; Houtepen, A. J.; Boehme, S.; de Mello Donegá, C.; Vanmaekelbergh, D.; Bonn, M. Spectroscopic Studies of Electron Injection in Quantum Dot Sensitized Mesoporous Oxide Films. *J. Phys. Chem. C* **2010,** *114*, 18866–18873.
41. Prasittichai, C.; Hupp, J. T. Surface Modification of SnO_2 Photoelectrodes in Dye-Sensitized Solar Cells: Significant Improvements in Photovoltage *via* Al_2O_3 Atomic Layer Deposition. *J. Phys. Chem. Lett.* **2010,** *1*, 1611–1615.
42. Yang, S. M.; Huang, C. H.; Zhai, J.; Wang, Z. S.; Jiang, L. High Photostability and Quantum Yield of Nanoporous TiO_2 thin Film Electrodes Co-sensitized with Capped Sulfides. *J. Mater. Chem.* **2002,** *12*, 1459–1464.
43. Diguna, L. J.; Shen, Q.; Kobayashi, J.; Toyoda, T. High Efficiency of CdSe Quantum-Dot-Sensitized TiO_2 Inverse Opal Solar Cells. *Appl. Phys. Lett.* **2007,** *91*, 023116-3.
44. Barea, E. M.; Shalom, M.; Giménez, S.; Hod, I.; Mora-Seró, I. n.; Zaban, A.; Bisquert, J. Design of Injection and Recombination in Quantum Dot Sensitized Solar Cells. *J. Am. Chem. Soc.* **2010,** *132*, 6834–6839.
45. Bisquert, J. Theory of the Impedance of Electron Diffusion and Recombination in a Thin Layer. *J. Phys. Chem. B* **2002,** *106*, 325–333.
46. Halme, J.; Boschloo, G.; Hagfeldt, A.; Lund, P. Spectral Characteristics of Light Harvesting, Electron Injection, and Steady-State Charge Collection in Pressed TiO_2 Dye Solar Cells. *J. Phys. Chem. C* **2008,** *112*, 5623–5637.
47. Lobato, K.; Peter, L. M.; Würfel, U. Direct Measurement of the Internal Electron Quasi-Fermi Level in Dye Sensitized Solar Cells Using a Titanium Secondary Electrode. *J. Phys. Chem. B* **2006,** *110*, 16201–16204.
48. Peter, L. M. Dye-Sensitized Nanocrystalline Solar Cells. *Phys. Chem. Chem. Phys.* **2007,** *9*, 2630–2642.
49. Jennings, J. R.; Peter, L. M. A Reappraisal of the Electron Diffusion Length in Solid-State Dye-Sensitized Solar Cells. *J. Phys. Chem. C* **2007,** *111*, 16100–16104.
50. Enright, B.; Fitzmaurice, D. Spectroscopic Determination of Electron and Hole Effective Masses in a Nanocrystalline Semiconductor Film. *J. Phys. Chem.* **1996,** *100*, 1027–1035.
51. Button, K. J.; Fonstad, C. G.; Dreybrodt, W. Determination of the Electron Masses in Stannic Oxide by Submillimeter Cyclotron Resonance. *Phys. Rev. B* **1971,** *4*, 4539–4542.
52. Ito, S.; Murakami, T. N.; Comte, P.; Liska, P.; Grätzel, C.; Nazeeruddin, M. K.; Grätzel, M. Fabrication of Thin Film Dye Sensitized Solar Cells with Solar to Electric Power Conversion Efficiency over 10%. *Thin Solid Films* **2008,** *516*, 4613–4619.
53. Hodes, G.; Manassen, J.; Cahen, D. Electrocatalytic Electrodes for the Polysulfide Redox System. *J. Electrochem. Soc.* **1980,** *127*, 544–549.
54. Giménez, S.; Mora-Seró, I.; Macor, L.; Guijarro, N.; Lana-Villarreal, T.; Gómez, R.; Diguna, L. J.; Shen, Q.; Toyoda, T.; Bisquert, J. Improving the Performance of Colloidal Quantum-Dot-Sensitized Solar Cells. *Nanotechnology* **2009,** *20*, 295204.